Electronic Supplementary Material (ESI) for Journal of Materials Chemistry C.

Supporting Information

Biomimetic engineering spider silk fibres with graphene for electric devices with humidity and motion sensitivity

Xiankai Li,[a,b] Lu Zong,[a,b] Xiaochen Wu,[a] Jun You,[a] Mingjie Li[a] and Chaoxu Li,*[a,b]

[a.] Group of Biomimetic Smart Materials, CAS Key Lab of Bio-based Materials
Qingdao Institute of Bioenergy and Bioprocess Technology, Chinese Academy of Sciences
Songling Road 189, Qingdao 266101, P. R. China

[b.] University of Chinese Academy of Sciences, 19A Yuquan Road, Beijing 100049, P. R. China

*E-mail: licx@qibebt.ac.cn.

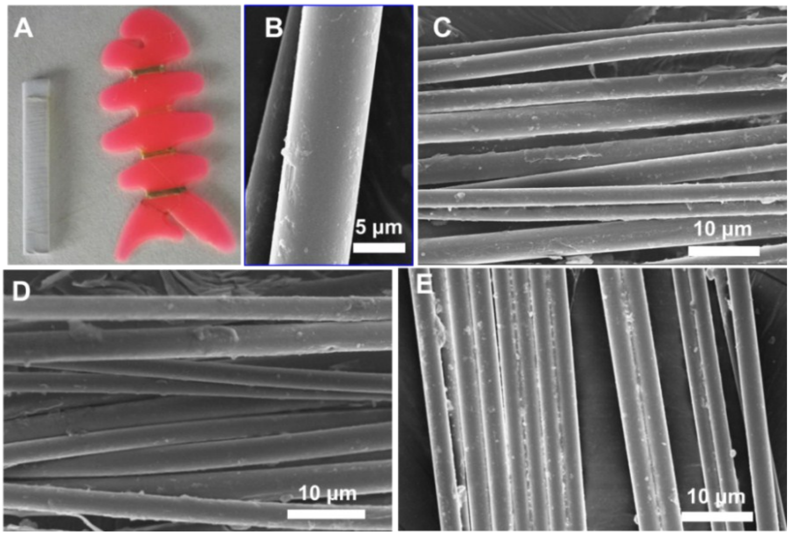

Fig. S1 (A) Dragline of *Nephila clavita* twined on paperboard and fishline bobbin. (B-E) Typical SEM images of spider silk fibres.

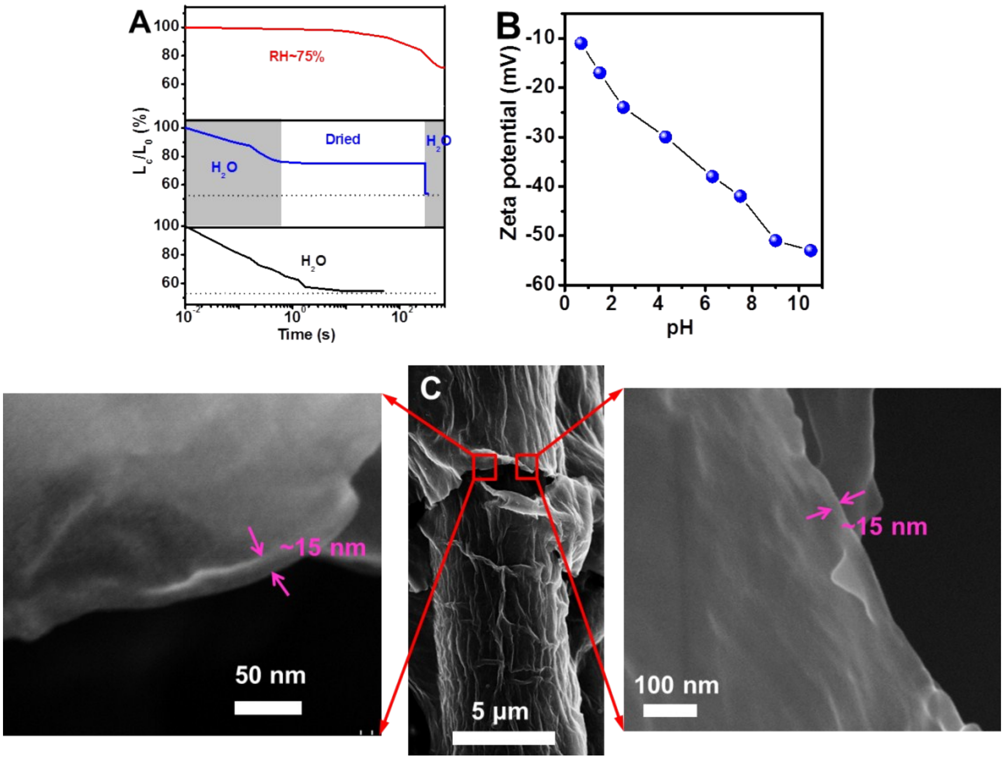

Fig. S2 (A) Supercontraction kinetics of natural spidroin fibres under different relative humidity. L_0 is initial length of spidroin fibre. (B) Zeta potential of GO solution at different pH values (detected by Delsa^{TM} Nano C particle analyser, Beckman Coulter, USA). (C) SEM image showing thickness of graphene sheath.

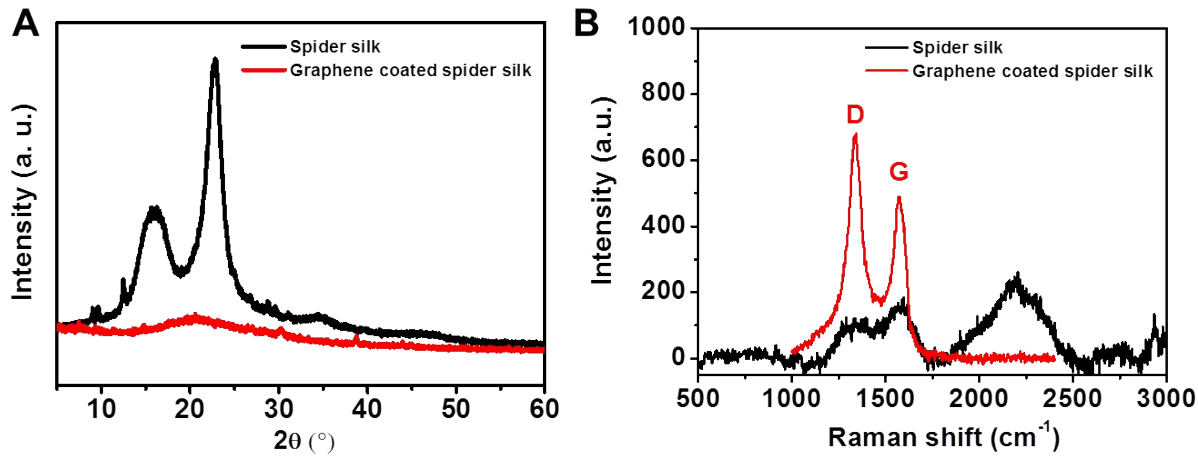

Fig. S3 (A) XRD and (B) Raman patterns of natural spidroin fibre and graphene-coated spidroin fibres with wrinkles.

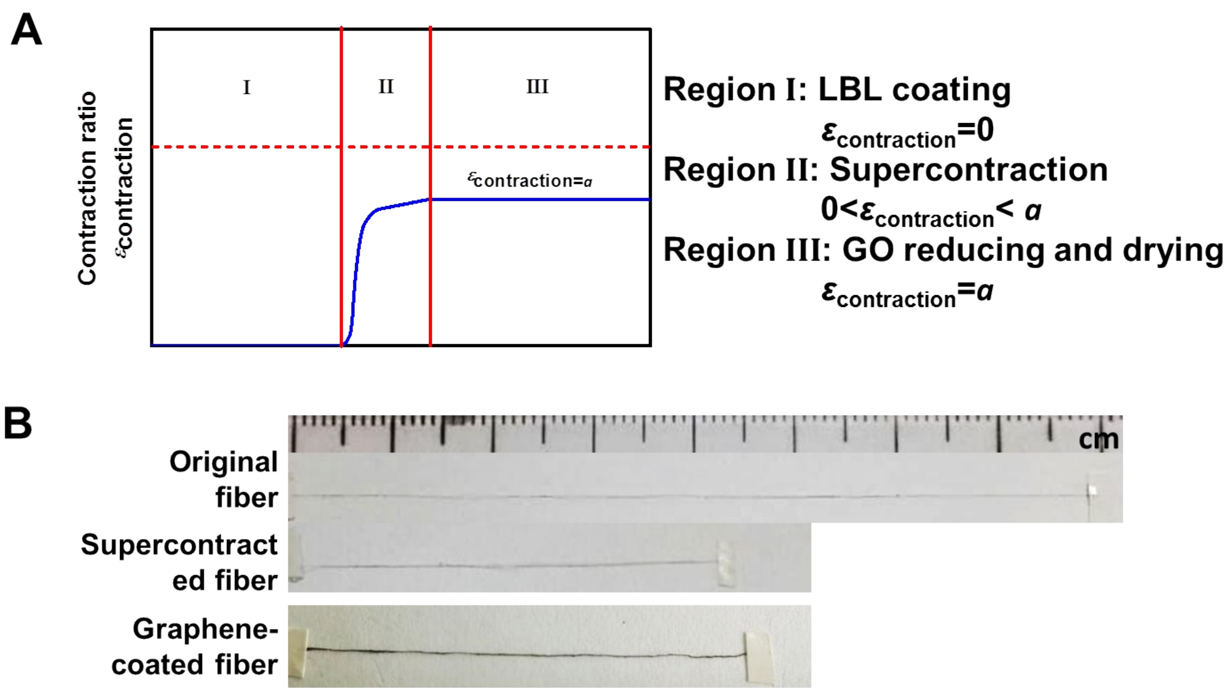

Fig. S4 (A) Variation of supercontraction ratio in three-step production procedure of graphene-coated spidroin fibres with wrinkles. (B) Visual comparison of natural spidroin fibres, supercontracted spidroin fibres and graphene-coated spidroin fibres with wrinkles.

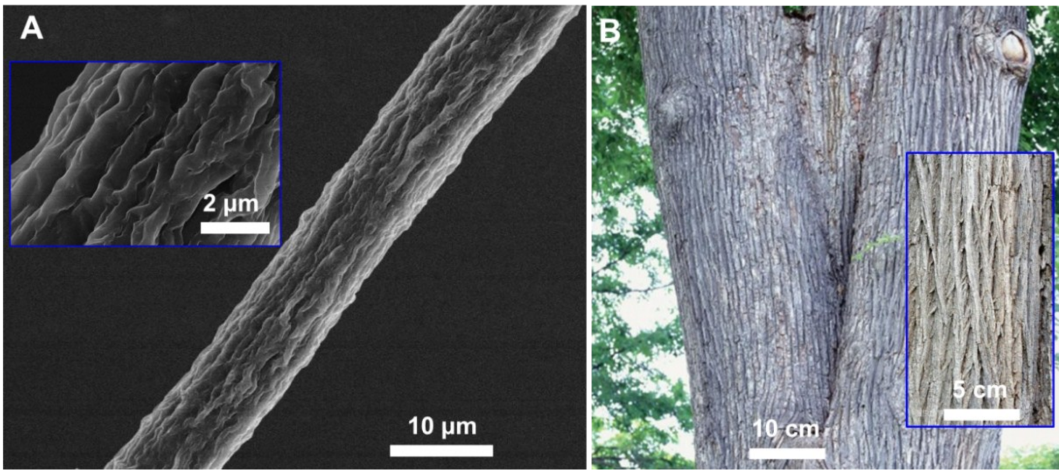

Fig. S5 (A) SEM image of graphene-coated spidroin fibres with wrinkles but without supercontraction. (B) Elm bark.

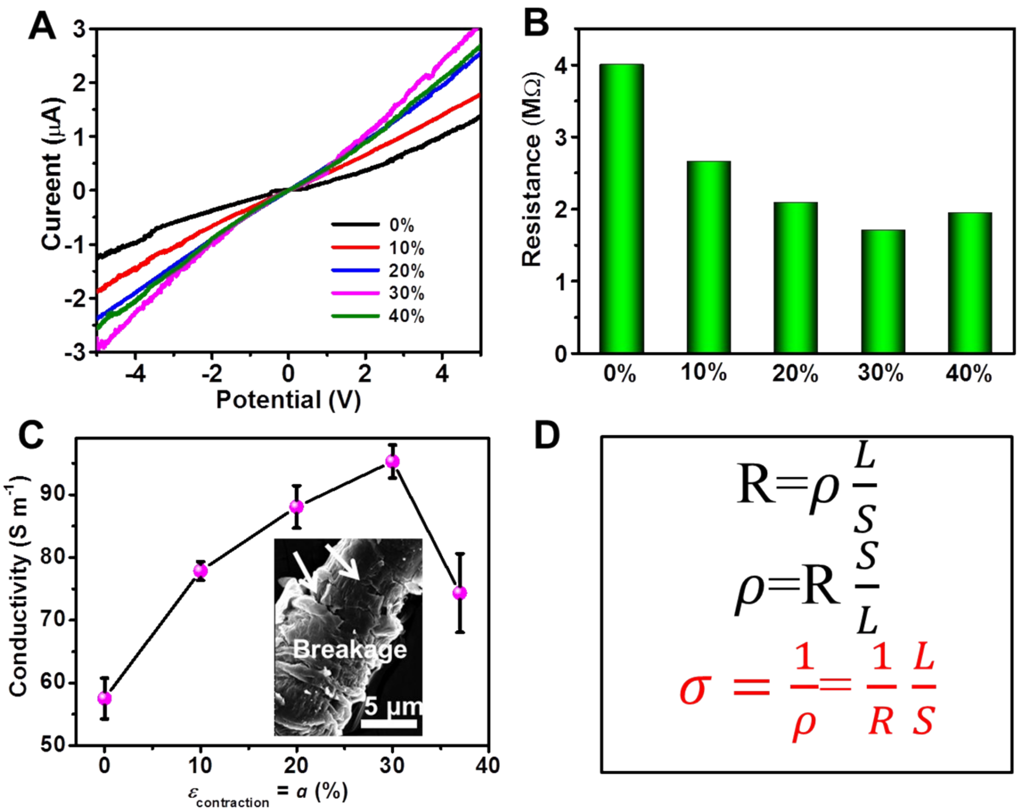

Fig. S6 Electric evaluation of graphene-coated spidroin fibres with different wrinkle degrees. Wrinkle degree was controlled by $\varepsilon_{contraction}=a$ value during the production procedure. (A) Current-voltage curves; (B) Calculated electric resistance; (C) Conductivity; (D) Calculation equations. (R: resistance; L: length of the fibre; S: cross section area of the fibre; ρ: electric resistivity; σ: electrical conductivity)

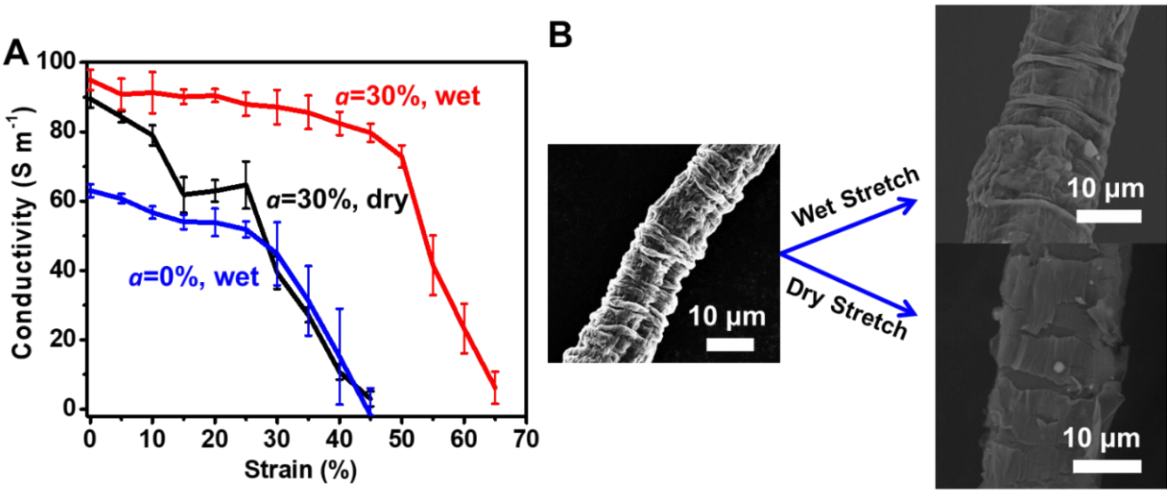

Fig. S7 (A) Dependence of electric conductivity on strain and wrinkle degree for graphene-coated spidroin fibres. Wrinkle degree was controlled by $\varepsilon_{contraction}=a$ value during the production procedure. (B) Wrinkle variation during wet stretching and dry stretching processes.

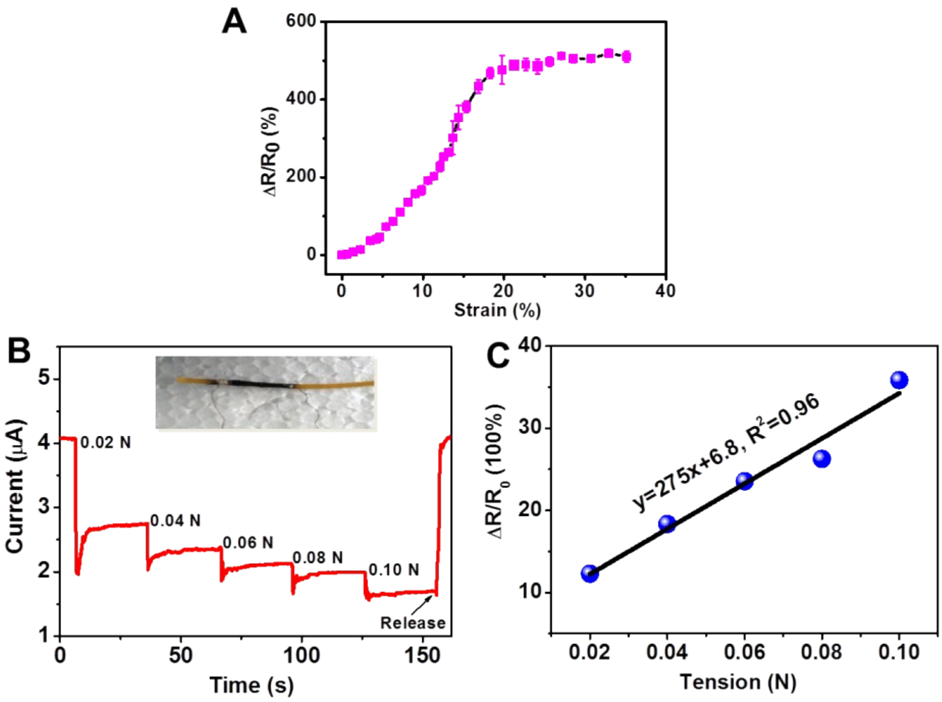

Fig. S8 (A) Dependence of relative resistance on strain. (B & C) Responsivity of electric current to force (B) and tensions (C). Electric modulus of rubber band (diameter ~2mm): ~500 kPa.

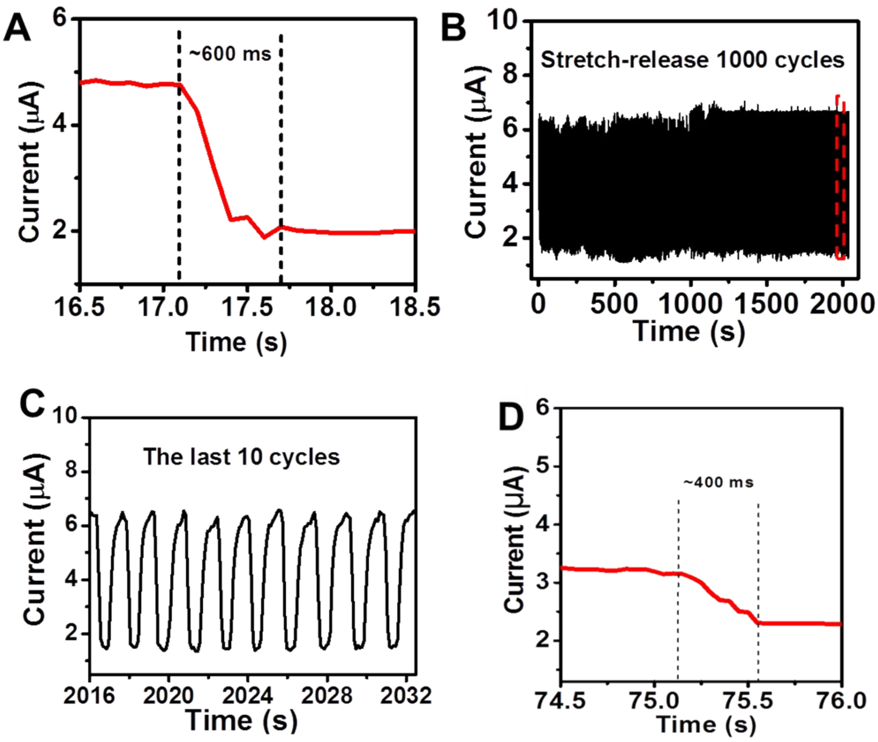

Fig. S9 (A) Repaid response of tendril-like sensor with 10% strain. (B) Stability of tendril-like sensor under stretch-release cycle. Strain: 13%. (C) The current change curves of the last 10 cycles cycles extracted from the red part in (B). (D) Rapid response of tendril-like sensor under 45° finger bending.

Sensing mechanism of the tendril-like sensor during stretching:

SEBS diameter, 2*R*=1.5 mm; silk fiber diameter, 2*r*=0.095 mm; initial length of SEBS rod, *H*=10 mm; maximum length of SEBS rod during sensing, *H*'=11.37 mm.

Here, the conductive silk fiber was wrapped on the SEBS rod turn-by-turn compactly, so the length of silk fiber in each turn could be calculated by:

$$l = 2\pi R = 4.71\ mm$$

The number of turns, *N*, wrapped could be evaluated as:

$$N = H/2r \approx 105$$

Therefore, the length variation, Δh, of SEBS rod in each turn during sensing at the maximum could be calculated as:

$$\Delta h = \frac{H - H'}{N} \approx 0.013\ mm$$

So, the length variation of conductive silk fiber, *l'*, in each turn could be calculated by unfolding the cylindrical surface in each turn:

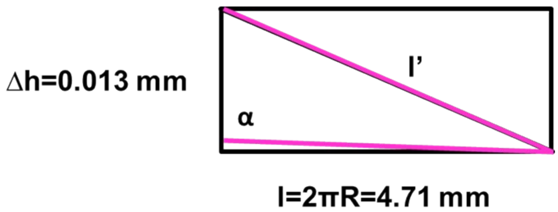

where angle $\alpha \approx 90°$, and *l'* could be calculated by:

$$l' = \sqrt{l^2 + \Delta h^2} = 4.710018 \text{ mm}$$

Therefore the length variation ratio of the whole conductive silk fiber could be calculated:

$$\frac{l' - l}{l} * 100\% = 3.8 * 10^{-4}\%$$

So the length variation ratio of the conductive silk fiber was very low, and the variation of ripples on the conductive silk fiber was also very very small. Based on the above analysis, most of the contribution to the resistance variation should be from fibre separation during stretching.

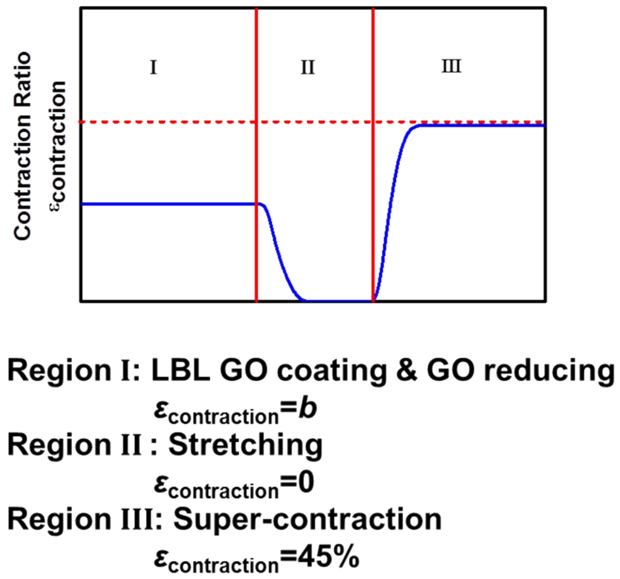

Fig. S10 Variation of supercontraction ratio in three-step production procedure of graphene-coated spidroin fibres with overlapped cracks.

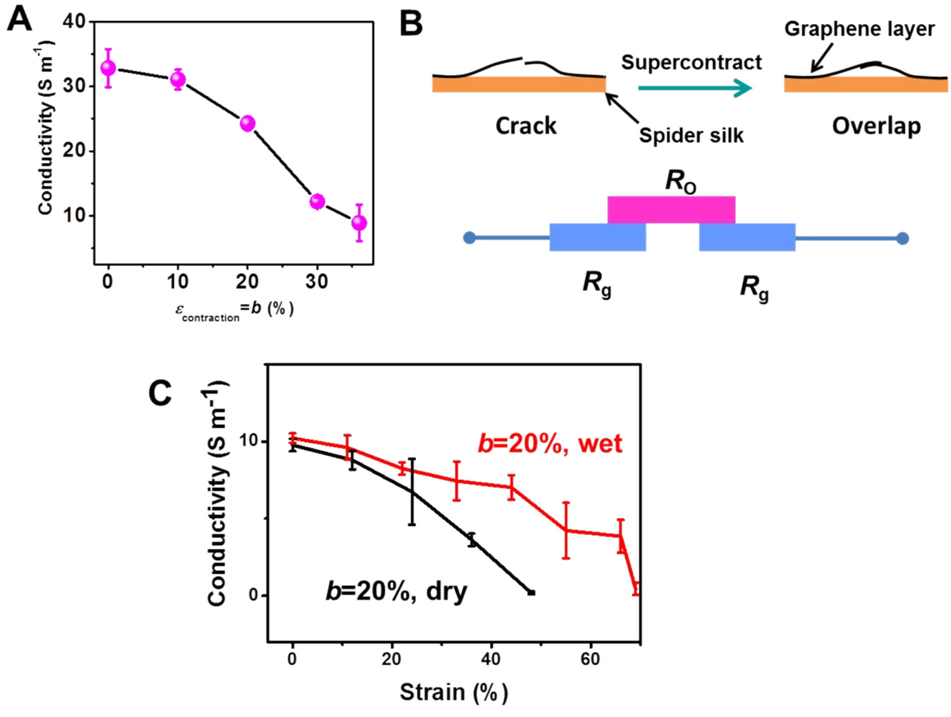

Fig. S11 (A) Electric conductivity of graphene-coated spidroin fibres with different degree of overlapped cracks. Overlapped cracks were controlled by $\varepsilon_{contraction}=b$ value during the production procedure. (B) Schematic illustration of variation of overlapped cracks during stretching. R_g is inherent resistance of graphene sheath; R_O is resistance resulted by overlap. (C) Dependence of electric conductivity on strain under dry and wet conditions. Cracks were produced with $\varepsilon_{contraction}=b$ ~20%.

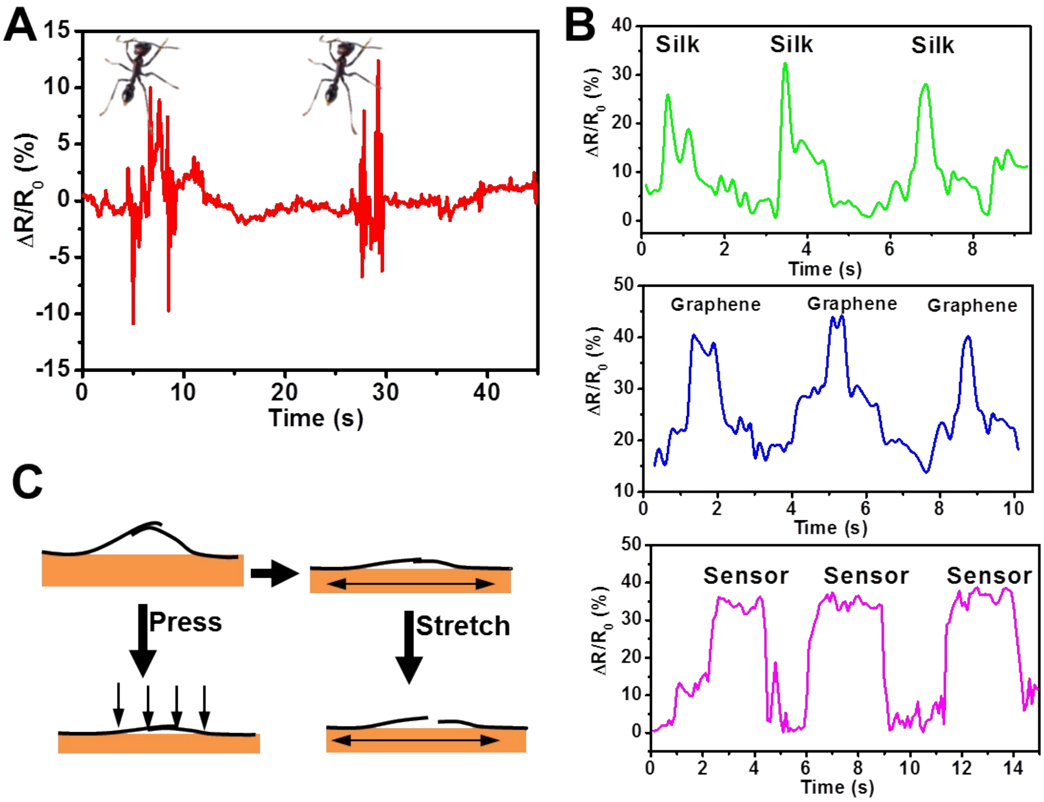

Fig. S12 (A) Responsivity of relative electric resistance of vibration sensor to ant motion. (B) Responsivity of relative electric resistance of vibration sensor to throat vibration during speaking different words. (C) Schematic illustration of variation of overlapped cracks during stretching and pressure.

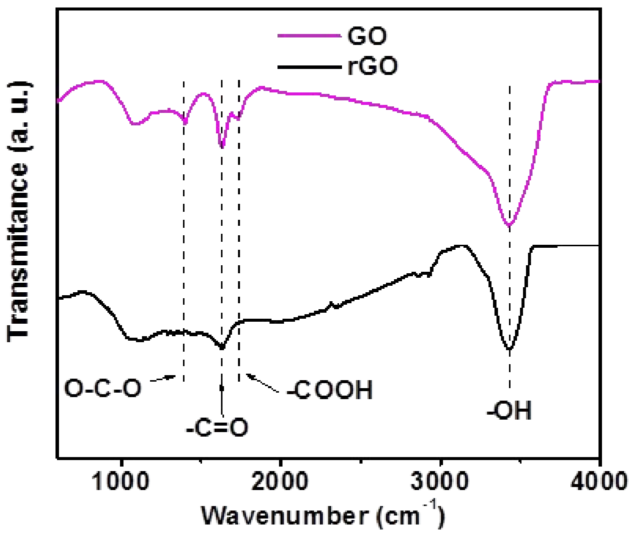

Fig. S13 FTIR spectra of GO and chemically reduced GO (rGO).